Journal of Photochemistry and Photobiology B: Biology 121 (2013) 75–85

Contents lists available at SciVerse ScienceDirect

Journal of Photochemistry and Photobiology B: Biology

journal homepage: www.elsevier.com/locate/jphotobiol

Synthesis, characterization and *in vitro* DNA binding and cleavage studies of Cu(II)/Zn(II) dipeptide complexes

Farukh Arjmand [a,*], A. Jamsheera [a], D.K. Mohapatra [b]

[a] Department of Chemistry, Aligarh Muslim University, Aligarh 202 002, Uttar Pradesh, India
[b] Diversity Oriented Synthesis Laboratory, Indian Institute of Chemical Technology, Hyderabad 500 607, Andhra Pradesh, India

ARTICLE INFO

Article history:
Received 29 August 2012
Received in revised form 29 November 2012
Accepted 19 December 2012
Available online 26 February 2013

Keywords:
Dipeptide Cu(II) and Zn(II) complexes
DNA binding profile
pBR322 DNA cleavage
In vitro anticancer activity

ABSTRACT

Novel dipeptide complexes Cu(II)·Val-Pro (**1**), Zn(II)·Val-Pro (**2**), Cu(II)·Ala-Pro (**3**) and Zn(II)·Ala-Pro (**4**) were synthesized and thoroughly characterized using different spectroscopic techniques including elemental analyses, IR, NMR, ESI–MS and molar conductance measurements. The solution stability study carried out by UV–vis absorption titration over a broad range of pH proved the stability of the complexes in solution. *In vitro* DNA binding studies of complexes **1–4** carried out employing absorption, fluorescence, circular dichroism and viscometric studies revealed the binding of complexes to DNA via groove binding. UV–vis titrations of **1–4** with mononucleotides of interest viz., 5′-GMP and 5′-TMP were also carried out. The DNA cleavage activity of the complexes **1** and **2** were ascertained by gel electrophoresis assay which revealed that the complexes are good DNA cleavage agents and the cleavage mechanism involved a hydrolytic pathway. Furthermore, *in vitro* antitumor activity of complex **1** was screened against human cancer cell lines of different histological origin.

1. Introduction

Small molecules binding to specific sites along DNA molecule are considered as potential chemotherapeutic agents. Peptides are attracting much attention since Novartis launched a vasopressin drug analog Lypressin in 1970, presently ca. 30 peptides have been marketed as key classes of therapeutics. Their role as mediators of key biological functions and their unique intrinsic properties make them particularly attractive therapeutic agents. They can surmount the hurdles of present cancer chemotherapeutic drugs including, little unspecific binding to molecular structures other than the desired target, minimization of drug–drug interactions and less accumulation in tissues reducing risks of complications due to intermediate metabolites. The fact that peptides affect the tumor cells rapidly and that their secondary metabolites are free amino acids proves that the peptides have minimized side effects as compared to other chemotherapeutic agents that are available currently. Recently, it has been reported that some peptide derivatives show antitumor activity with little toxicity against non-malignant cells either by triggering apoptosis [1,2] or by forming ion channels/pores [3]. Furthermore, some peptides were found to be cytotoxic against MDR cancer cells [4,5].

Peptides are versatile and powerful ligands for a range of metal ions since they contain a variety of potential donor centers. Metallopeptide systems are unique and can affect the biological activity of peptides. Metals may be directly bound into peptides and have been used for DNA selective recognition and/or cleavage [6,7]. It was reported that peptide fictionalization of polypyridyl ruthenium(II) [8,9] or rhodium(III) [10,11] metallo-intercalators improved the selectivity of the parent intercalators, with similar effects observed by conjugating minor groove binders with short peptides that mimic natural protein motifs [12].

The rationale of our strategy is to design peptide–metal complexes which prove to possess pronounced biological and better pharmacological activity. Amongst the metal ions chosen, we have opted for biocompatible endogenous metal ions Cu and Zn, known for their essential role in biological living system. In particular, the complexes based on essential metals are less toxic than those with non-essential ones. Cu(II) complexes are known to play a significant role either in naturally occurring biological systems or as pharmacological agents [13,14] whereas the importance of zinc for stabilization of protein loops in enzymes, zinc fingers, etc., has generated new interest in the field of Zn coordination chemistry [15,16]. The discovery of the ‘zinc fingers’ has triggered intensive research on the interaction of proteins with Zn ions [17,18]. The investigation of Cu(II)/Zn(II)-peptide complexes is of scientific and technological importance, since such systems may be regarded as models for both protein–DNA and antitumor agent-DNA interactions.

Herein we report, the synthesis, spectroscopic characterization, DNA binding and cleavage studies of dipeptide complexes of Cu(II) and Zn(II). The synthetic strategy involves peptide moiety as a scaffold for our complexes thereby, these complexes would exhibit desirable therapeutic properties for more efficacious and safer drug

* Corresponding author. Tel.: +91 571 2703893.
E-mail address: farukh_arjmand@yahoo.co.in (F. Arjmand).

1011-1344/$ - see front matter © 2013 Elsevier B.V. All rights reserved.
http://dx.doi.org/10.1016/j.jphotobiol.2012.12.009

administration owing to (a) better cellular uptake, (b) improved aqueous solubility, (c) selectivity and specificity towards the target at the molecular level and (d) reduced toxicity due to biocompatible endogenously friendly ligand and metal ions. *In vitro* DNA binding studies revealed that these complexes are avid DNA binding agents; thereby they can act as potent chemotherapeutics. Furthermore, DNA cleavage activity of **1** and **2** with pBR322 DNA has been carried out, in addition *in vitro* cytotoxicity of complex **1** was tested against various human cancer cell lines.

2. Experimental

2.1. Materials

Alanine, Valine, Proline, HOBT (N-Hydroxybenzotriazole) (SRL), $Cu(NO_3)_2{\cdot}3H_2O$, $Zn(NO_3)_2{\cdot}6H_2O$ (Ranchem), EDCI (1-Ethyl-3-(3-dimethylaminopropyl)carbodiimide Hydrochloride), Boc anhydride, $SOCl_2$, TFA (trifluro acetic acid), calf thymus DNA (CT-DNA), ascorbic acid (Merck), H_2O_2, 3-mercaptopropionic acid, glutathione, methyl green, DAPI, tertiary butyl alcohol, sodium azide, superoxide dismutase (Sigma), guanosine-5′-monophosphate disodium salt (5′-GMP) and thymidine-5′-monophosphate disodium salt (5′-TMP) (Fluka) were used without further purification.

2.2. Methods and instrumentation

Elemental analyses were performed on Elementar Vario EL III. Fourier transform infrared spectra were recorded on Interspec 2020 FTIR spectrometer in Nujol. ^{1}H NMR spectra was obtained on a Bruker DRX-400 spectrometer. Electrospray mass spectra were recorded on Micromass Quattro II triple quadrupol mass spectrometer. EPR spectra of the copper complexes were recorded on a Varian E 112 spectrometer at the X-band frequency (9.1 GHz) at LNT. Molar conductance was measured at room temperature on a Digisun Electronic Conductivity Bridge. Electronic spectra were recorded on a UV-1700 PharmaSpec UV–visible Spectrophotometer. Fluorescence measurements were made on Hitachi F-2500 Fluorescence Spectrophotometer. CD spectra were recorded on Applied Photophysics Chirascan Circular Dichroism Spectrometer with Stop Flow. Viscosity measurements were carried out from observed flow time of CT-DNA containing solution ($t > 100$ s) corrected for the flow time of buffer alone (t_0), using Ostwald's Viscometer at 25 ± 0.01 °C. Flow time was measured with a digital stopwatch.

DNA binding experiments which include absorption spectral traces, luminescence, circular dichroism and viscosity experiments conformed to the standard methods [19,20] and practices previously adopted by our laboratory [21]. While measuring the absorption spectra an equal amount of DNA was added to both the compound solution and the reference solution to eliminate the absorbance of the CT-DNA itself, and the CD contribution by the CT-DNA and Tris buffer was subtracted through base line correction.

2.2.1. In vitro antitumor studies

The cell lines used for *in vitro* antitumor screening activity were A498 (Renal cell), A549 (Lung), Zr-75-1 (Breast), HT29 (Colon adenocarcinoma grade II cell line), A2780 (Ovary), SiHa (Uterine cervix) and MCF7 (Human breast). These human malignant cell lines were procured and grown in RPMI-1640 medium supplemented with 10% Fetal Bovine Serum (FBS) and antibiotics to study growth pattern of these cells. The proliferation of the cells upon treatment with chemotherapy was determined using the Sulforhodamine B (SRB) semi automated assay [22]. Cells were seeded in 96 well plates at an appropriate cell density to give optical density in the linear range (from 0.5 to 1.8) and were incubated at 37 °C in CO_2 incubator for 24 h. Stock solutions of the complexes were prepared as 100 mg/mL in DMSO and four dilutions i.e. 10 μL, 20 μL, 40 μL, 80 μL, in triplicates were tested, each well receiving 90 μL of cell suspension and 10 μL of the drug solution. Appropriate positive control (Adriamycin) and vehicle controls were also run. The plates with cells were incubated in CO_2 incubator with 5% CO_2 for 24 h followed by drug addition. The plates were incubated further for 48 h. Termination of experiment was done by gently layering the cells with 50 μL of chilled 30% TCA (in case of adherent cells) and 50% TCA (in case of suspension cell lines) for cell fixation and kept at 4 °C for 1 h. Plates were stained with 50 μL of 0.4% SRB for 20 min. The bound SRB was eluted by adding 100 μL 10 mM Tris (pH 10.5) to each of the wells. The absorbance was read at 540 nm with 690 nm as reference wave length. All the experiments were repeated three times.

2.3. Syntheses

2.3.1. Synthesis of dipeptides (L_1, L_2)

The dipeptides used in this study were synthesized by conventional solution phase methodology [23]. The Boc group was used for N-terminal protection and the C-terminus was protected as a methyl ester. Coupling reactions were mediated by EDCI-HOBT.

Boc-amino acid (10 mmol) was dissolved in dichloromethane (DCM, 20 mL). To this solution, EDCI (4.77 g, 25 mmol) was added at 0 °C and the reaction mixture was stirred for 15 min amino acid methylester (10 mmol) was added followed by HOBT (2.74 g, 20 mmol) to the above reaction mixture under stirring. After 24 h, the reaction mixture was filtered; the residue was washed with DCM (30 mL) and added to the filtrate. The filtrate was washed with 5% sodium bicarbonate and saturated sodium chloride solutions. The organic layer was dried over anhydrous Na_2SO_4, filtered and evaporated under reduced pressure. The crude product was purified by column chromatography.

L_1 Semisolid mass; Yield 63.7%; IR (Nujol, cm^{-1}): 3315 (νNH); 1716 (νC═O); 1617 (ν_{as}O—C═O); 1455 (ν_sO—C═O). ^{1}H NMR ($CDCl_3$, ppm): 5.20 (1H, —NH, Boc), 4.50 (1H, m, —CH, Val), 4.25 (1H, t, —CH, Pro), 3.80 (2H, t, —CH_2, Pro), 3.71 (3H, s, —OCH_3), 2.00 (2H, m, —CH_2, Pro), 2.25 (2H, m, —CH_2, Pro), 1.00 (3H, d, —CH_3, Val), 1.45 (9H, s, *t*Butyl group). ESI–MS (*m*/*z*): 329 $[C_{16}H_{28}N_2O_5 + H]^+$.

L_2 Semisolid mass; Yield 67.2%; IR (Nujol, cm^{-1}): 3317 (νNH); 1714 (νC═O); 1650 (ν_{as}O—C═O); 1443 (ν_sO—C═O). ^{1}H NMR ($CDCl_3$, ppm): 5.35 (1H, —NH, Boc), 4.51 (1H, m, —CH, Ala), 4.45 (1H, t, —CH, Pro), 3.61 (2H, t, —CH_2, Pro), 3.70 (3H, s, —OCH_3), 2.00 (2H, m, —CH_2, Pro), 2.25 (2H, m, —CH_2, Pro), 1.35 (3H, d, —CH_3, Ala), 1.45 (9H, s, *t*Butyl group). ESI–MS (*m*/*z*): 301 $[C_{14}H_{24}N_2O_5 + H]^+$.

2.3.2. Synthesis of Cu(II)·Val-Pro (**1**)

The dipeptide, L_1 (0.43 g, 2 mmol) was dissolved in minimum amount (15 mL) of absolute methanol. To this a methanolic solution of $Cu(NO_3)_2{\cdot}3H_2O$ (0.24 g, 1 mmol) was added. The solution was stirred for 1 h. The resultant pale blue solution was left for slow evaporation at room temperature. The blue precipitate obtained was filtered, washed with petroleum ether and dried in vacuo (Scheme 1).

Yield, 66.7%. IR (Nujol, cm^{-1}): 3218 (νNH); 1674 (νC═O); 1674 (ν_{as}O—C═O); 1408 (ν_sO—C═O); 452 (Cu—N); 519 (Cu—O). ESI–MS (*m*/*z*): 491 $[C_{20}H_{34}N_4O_6Cu + H]^+$. Molar Conductance, Λ_M (1×10^{-3} M, DMSO): 32.7 Ω^{-1} cm^2 mol^{-1} (non-electrolyte). UV–vis (DMSO, nm): 257, 645 nm. Anal. Calc. (%) (for $C_{20}H_{34}N_4O_6$-Cu): C 49.02; H 6.99; N 11.43. Found (%): C 49.10; H 6.94; N 11.47.

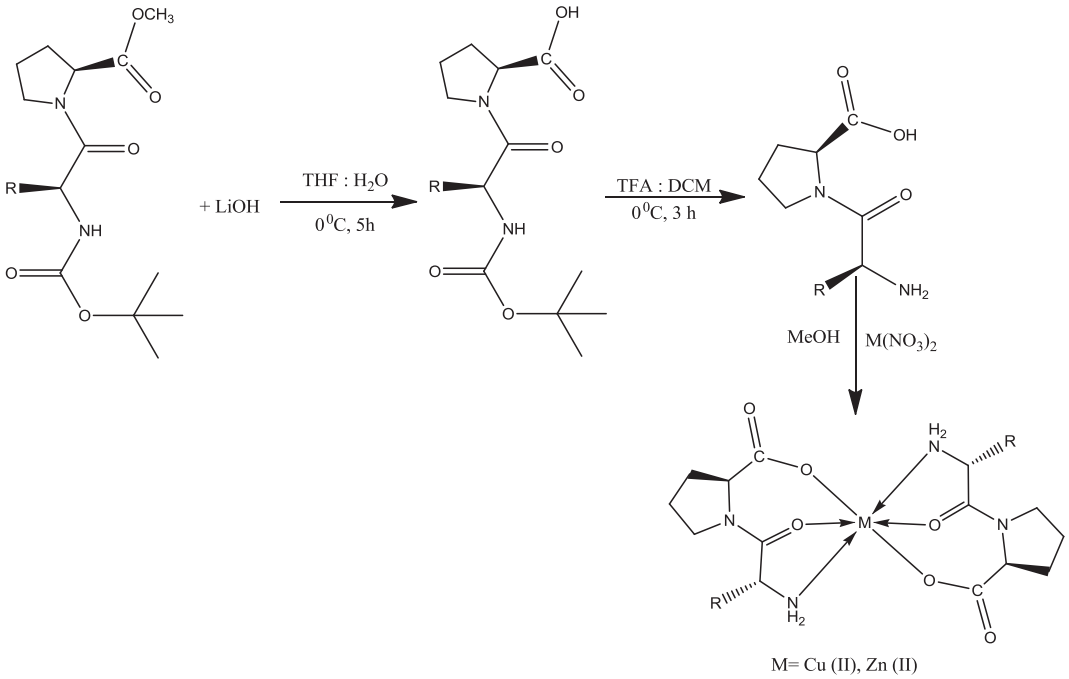

Scheme 1. Schematic representation of the synthesis of complexes **1**–**4**.

2.3.3. Synthesis of Zn(II)·Val-Pro(2)

This complex was synthesized by a similar procedure as described for **1** with a methanolic solution of $Zn(NO_3)_2{\cdot}6H_2O$ (0.29 g, 1 mmol).

Yield, 63.5%. IR (Nujol, cm^{-1}): 3188 (νNH); 1665 (νC═O); 1665 (ν_{as}O—C═O); 1394 (ν_sO—C═O); 464 (Zn—N); 512 (Zn—O). ^{1}H NMR (D_2O, ppm): 4.52 (2H, m, —CH, Val), 4.30 (2H, t, —CH, Pro), 4.15 (4H, t, —CH_2, Pro), 3.24 (4H, NH_2, Val), 2.35–2.00 (8H, m, —CH_2, Pro), 1.15 (6H, —CH_3, Val). ESI–MS (m/z): 491 $[C_{20}H_{34}N_4O_6Zn\text{-}H]^+$. Molar Conductance, Λ_M (1×10^{-3} M, DMSO): 30.6 Ω^{-1} cm^2 mol^{-1} (non-electrolyte). UV–vis (DMSO, nm): 258 nm. Anal. Calc. (%) (for $C_{20}H_{34}N_4O_6Zn$): C 48.84; H 6.97; N 11.39. Found (%): C 48.86; H 6.94; N 11.41.

*2.3.4. Synthesis of Cu(II)·Ala-Pro (**3**)*

The dipeptide, L_2 (0.37 g, 2 mmol) was dissolved in minimum amount (15 mL) of absolute methanol. To this a methanolic solution of $Cu(NO_3)_2{\cdot}3H_2O$ (0.24 g, 1 mmol) was added. The solution was stirred for 1 h. The blue precipitate appeared was filtered, washed with petroleum ether and dried in *vacuo*.

Yield, 62.35%. IR (Nujol, cm^{-1}): 3185 (νNH); 1668 (νC═O); 1652 (ν_{as}O—C═O); 1391 (ν_sO—C═O); 480 (Cu—N); 520 (Cu—O). ESI–MS (m/z): 439 $[C_{16}H_{26}N_4O_6Cu + 5H]^+$. Molar Conductance, Λ_M (1×10^{-3} M, DMSO): 33.1 Ω^{-1} cm^2 mol^{-1} (non-electrolyte). UV–vis (DMSO, nm): 256, 650 nm. Anal. Calc. (%) (for $C_{16}H_{26}N_4O_6Cu$): C 44.28; H 6.04; N 12.91. Found (%): C 44.29; H 6.00; N 12.89.

*2.3.5. Synthesis of Zn(II)·Ala-Pro (**4**)*

This complex was synthesized by a similar procedure as described for **3** with a methanolic solution of $Zn(NO_3)_2{\cdot}6H_2O$ (0.29 g, 1 mmol).

Yield, 64%. IR (Nujol, cm^{-1}): 3215 (νNH); 1667 (νC═O); 1667 (ν_{as}O—C═O); 1410 (ν_sO—C═O); 475 (Zn—N); 526 (Zn—O). ^{1}H NMR (D_2O, ppm): 4.58 (2H, m, —CH, Ala), 4.48 (2H, t, —CH, Pro), 3.24 (4H, NH_2, Val), 3.65 (4H, t, —CH_2, Pro), 2.45–2.10 (8H, m, —CH_2, Pro), 1.5 (6H, —CH_3, Ala). ESI–MS (m/z): 478 $[C_{16}H_{26}N_4O_6Zn + K + 3H]^+$. Molar Conductance, Λ_M (1×10^{-3} M, DMSO): 31.0 Ω^{-1} cm^2 mol^{-1} (non-electrolyte). UV–vis (DMSO, nm): 258 nm. Anal. Calc. (%) (for $C_{16}H_{26}N_4O_6Zn$): C 44.10; H 6.01; N 12.86. Found (%): C 44.11; H 6.03; N 12.89.

3. Results and discussion

3.1. IR spectra

Coordination behaviors of dipeptides to metal ions are delicately different among metals and peptides. The ν(NH) band at 3317 cm^{-1} in the free dipeptides appeared as a broad band at 3117–3215 cm^{-1} upon complexation. This change and relatively low frequency of $\nu(NH_2)$ bands assigned that terminal amino group of the peptide occupies one of the coordination sites of the metal ion [24]. The tertiary amide band at 1716 cm^{-1} has been shifted to low frequency upon complexation indicative of coordination of amide group to the central metal ion. A distinctive difference between the absorption of facial and meridional isomers was observed in the —C═O stretching region; the facial isomer has only one peak where as the meridional isomer has two split absorption peaks [25,26]. All the complexes exhibited a strong absorption around 1660 cm^{-1} with a shoulder band at 1530 cm^{-1} in the ν_{as}O—C═O region, indicating meridional geometry. ν_sO—C═O absorption band of the complexes was observed around 1400 cm^{-1}. The large difference (>200 cm^{-1}) between the two values designated the coordination of COO^- groups to the metal ion in a monodentate fashion [27]. Further evidence for complexation was provided by the presence of medium intensity bands around 455, 515 cm^{-1} corresponding to (Cu/Zn—N), (Cu/Zn—O), respectively in far IR region.

3.2. NMR spectra

The singlets at 1.45 and 3.70 ppm in the ^{1}H NMR spectra of ligands revealed the presence of *t-boc* and —$CO(OCH_3)$ group respectively in the ligands which disappeared upon deprotection with the emergence of a new resonance at 12.0–12.18 ppm corresponding to the —COOH group. The signals at 2.25 (multiplet), 3.80 (triplet) and 4.25 (triplet) ppm indicated the presence of proline moiety in

the ligands. A doublet at 1.0 and a triplet at 4.51 ppm revealed the presence of valine moiety in the ligand L_1 whereas a doublet at 1.35 and a quartet at 4.51 ppm revealed the presence of alanine in the ligand L_2.

Upon complexation the signals were shifted to downfield. The absence of —COOH resonance at 12.0–12.18 ppm in the complex indicated the coordination of carboxylic group to Zn through deprotonation. The NH_2 signal was shifted to 3.24 ppm in both the complexes indicating the involvement of amino group in complexation.

3.3. Mass spectra

Electrospray mass spectra in the positive ion mode were recorded for the free peptides and complexes **1**–**4**. ESI–MS spectra of the di-/tetra-peptides displayed prominent peaks at *m*/*z* 329, 301 and 469 corresponding to the fragments $[C_{16}H_{28}N_2O_5 + H]^+$, $[C_{14}H_{24}N_2O_5 + H]^+$ and $[C_{22}H_{36}N_4O_7 + H]^+$, respectively. Complex **1** displayed two peaks centered at *m*/*z* 491 and 215 corresponding to the fragments $[\mathbf{1} + H]^+$ and $[\mathbf{1}\text{-}C_{10}H_{17}N_2O_3Cu + 2H]^+$, respectively. Two major peaks are observed for complex **2** at *m*/*z* 491 and 215 corresponding to the fragments $[\mathbf{2}\text{-}H]^+$ and $[\mathbf{2}\text{-}C_{10}H_{17}N_2O_3\text{-}Zn + 2H]^+$, respectively. Complex **3** also displayed two prominent peaks at *m*/*z* 439 and 186 which could be assigned to $[\mathbf{3} + 5H]^+$ and $[\mathbf{3}\text{-}C_8H_{13}N_2O_3Cu + H]^+$, respectively. The peaks at *m*/*z* 478 and 187 in the spectrum of the complex **4** were assigned to $[\mathbf{4} + K + 3H]^+$ and $[\mathbf{4}\text{-}C_8H_{13}N_2O_3Zn + 2H]^+$, respectively.

3.4. EPR spectra

The EPR spectra of complexes **1** and **3** acquired at LNT under the magnetic field strength 3000 ± 1000*G* showed a spectrum, with both parallel and perpendicular *g* values. The EPR spectra of the complexes interpreted in terms of *g* values displayed $g_{||} = 2.313$, $g_{\perp} = 2.131$ and $g_{avg} = 2.894$ for complex **1** and $g_{||} = 2.338$, $g_{\perp} = 2.145$ and $g_{avg} = 2.921$ for complex **3** computed from the formula $g_{avg}^2 = g_{||}^2 + 2g_{\perp}^2/3$, suggested an octahedral geometry [28]. The trend $g_{||} > g_{\perp} > g_e$ (2.0023) revealed that the unpaired electron was located in the $d_x^2\text{-}d_y^2$ orbital of the Cu^{II} ions characteristic of axial symmetry. The parameter $G = (g_{||} - 2.0023)/(g_{\perp} - 2.0023)$, measures the exchange interaction between the metal center in a polycrystalline solid. $G > 4$ indicates negligible exchange interaction in the solid complex. For complexes **1** and **3** $G < 4$ indicated considerable exchange interaction in the complexes. For a Cu(II) complex, $g_{||}$ is a parameter sensitive enough to indicate covalence, $g_{||} < 2.3$ indicates a covalent complex whereas $g_{||} = 2.3$ or more for an ionic environment.

3.5. Electronic spectra

The electronic absorption spectra are often very helpful in the evaluation of results furnished by other methods of structural investigation. The UV–vis absorption spectra of the complexes **1**–**4** in DMSO were characterized by strong intra ligand absorption bands centered at 256–258 nm. The complexes exhibited charge transfer bands at 275–287 nm. The complexes **1** and **3** displayed d–d transition bands at 654 and 650 nm respectively. This spectral feature is typical of complexes in an octahedral coordination environment [29].

3.6. Solution stability studies

The stability of the complexes **1** and **3** were determined by UV–vis absorption titration at d–d band under identical conditions to those used for DNA binding studies in buffered solution at various pH values. UV–vis spectra of complexes **1** and **3** exhibited no change in the position of the d–d band over a pH range 2–12 with only minor change in intensity. The complexes also displayed similar spectra over a period of 24 h confirming the stability of the metal ion in the peptide metal complexes and also no precipitation was observed. The non-precipitation after 24 h time period and over a broad range of pH suggested the stability of the complexes in solution.

4. DNA binding studies

4.1. Electronic absorption studies

Electronic absorption spectroscopy is an effective method to examine the binding modes of the metal complexes with DNA. Upon addition of incremental amounts of CT-DNA ($0 - 0.2 \times 10^{-4}$ M), the absorption bands of the complexes (0.066×10^{-3} M) **1**–**4** exhibited hyperchromism (Fig. 1) without any shift in the intra ligand bands, suggesting that there exists a strong interaction between the complexes and DNA which is different from classical intercalation mode of binding, since intercalation involves hypochromism. The spectral changes of the complexes observed in presence of DNA can be rationalized in terms of groove binding [30]. The formation of DNA–peptide metal complex could induce changes in the spectral characteristics of both or either of DNA or peptide complexes [31]. Since DNA possesses several hydrogen bonding sites which are accessible in major and minor grooves, therefore, the complexes form hydrogen bonds via amine group of peptide moiety with N-3 of adenine or O-2 of thymine in the DNA, which may contribute to the hyperchromism observed in the absorption spectra.

In order to quantitatively evaluate the binding magnitude of the complexes **1**–**4** with DNA, the intrinsic binding constant k_b values of the complexes were determined from the spectral titration curves (Table 1). From the k_b values, it was found that all the dipeptide complexes show more or less similar binding affinity. The slight difference in binding behavior could be attributed to the chain length of peptides; which enhances the hydrophobicity, thereby resulting in higher binding affinity. The hydrophobic residues in peptides increase the stability of the peptide–DNA complex [32] and it is more likely that the hydrophobicity and the H-bonding ability of the peptide moiety can be responsible for the higher DNA binding affinity of complexes **1**–**4**, since the hydrophobic residues like Ala and Val can recognize the methyl on thymine base at major groove. It is worthwhile to mention that efficiency of this type of complexes in their biological studies has also been observed in earlier studies [33–35].

4.2. Interaction with 5′-GMP and 5′-TMP

Nucleotide–metal interactions have been reported to occur at nitrogen atom of the purine and pyrimidine rings as well as oxygen atom of the phosphate group present on the nucleotide [36]. Addition of increasing amounts of mononucleotides (5′-GMP and 5′-TMP) to the complexes **1**–**4** resulted in hyperchromism (Figs. 2a and 2b) without any substantial change in the position of the IL band of the complexes validating interaction of the complexes to different nucleotides. These spectral changes upon addition of increasing amounts of mononucleotides authenticate the strong interaction of complexes to nucleotides through electrostatic surface interactions, preferably via groove binding. Metal ions promote hydrophobic interaction between nucleotides and amino acids, and mediate interaction between proteins and nucleic acids through formation of ternary complexes. The purine and pyrimidine bases of CT-DNA become exposed due to the unwinding of the DNA helix promoting an effective binding to these base pairs with the transition metal complexes.

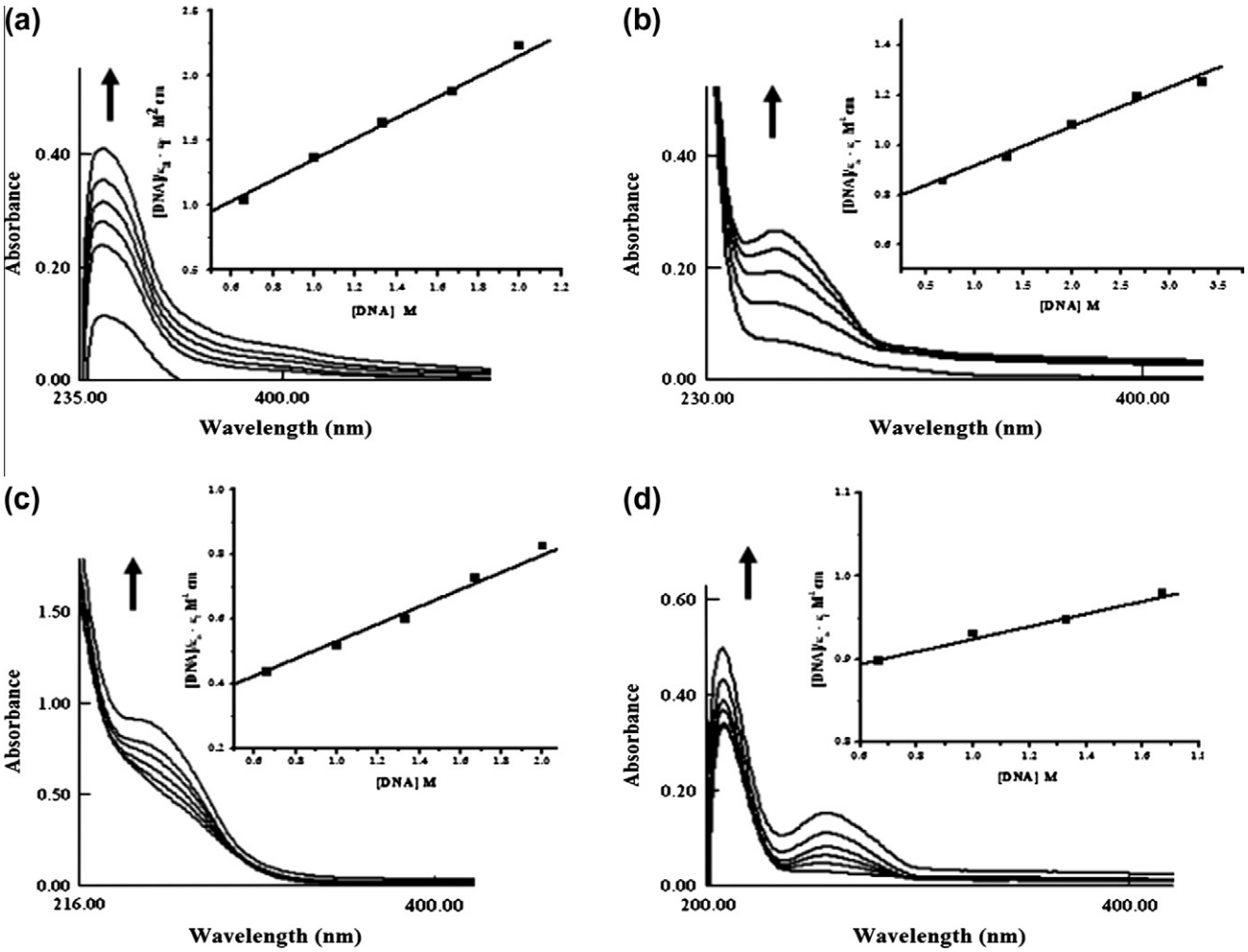

Fig. 1. UV–vis absorption spectra of complexes **1** (a), **2** (b), **3** (c) and **4** (d) in Tris HCl buffer (0.01 M, pH 7.2) upon addition of CT-DNA. Arrows indicate the change in absorbance upon increasing DNA concentration. Inset: Plots of [DNA] vs. [DNA]/ε_a–ε_f for the titration of CT-DNA with complexes.

Table 1
The binding constant (K_b) values of complexes with the DNA (mean standard deviation of ±0.12).

Complex	K_b (M^{-1})	Monitored at (nm)	% Hyperchromism
1	7.70×10^4	257	29
2	1.90×10^4	258	25
3	6.50×10^4	256	27
4	9.90×10^3	258	26

To compare quantitatively the affinity of the complexes to mononucleotides, the intrinsic binding constant (k_b) was also determined (Table 2). The binding constants clearly revealed selectivity for nucleobases – a higher binding propensity of Cu(II) complexes for 5′-GMP while Zn(II) complexes preferentially binds to 5′-TMP. The higher propensity of Cu(II) complexes to 5′-GMP could be attributed to preferential binding of the complexes to the N7 nitrogen of 5′-GMP occurring due to the thermodynamic and kinetic stability of guanine residue [37]. While in Zn(II) complexes hydrogen bonds could be favored between nitrogen atoms of ligand with carbonyl oxygen of thymine. Furthermore, the presence of electron withdrawing two oxo groups at the C2 and C3 position of the thymine lowers the energy of the lone pair orbital at N3 of thymine base which results in stronger molecular orbital interaction in comparison to guanine resulting in preferential binding of Zn(II) towards thymine [38].

4.3. Fluorescence spectral studies

To further confirm the interaction between the complexes and CT-DNA, emission experiments were carried out. At room temperature, **1**–**4** exhibited emission bands at 390 nm when excited at 260 nm (Fig. 3). Upon addition of increasing amounts of CT-DNA to fixed amount of complexes, the fluorescence emission intensity was enhanced indicating the strong interaction of complexes with DNA. Hydrophobic interactions between the complexes and polyelectrolyte may induce changes in the excited state properties either due to electrostatic association or intercalation [39]. Although the emission enhancement could not be regarded as a criterion for binding mode, they are related to the extent to which the complex gets into the hydrophobic environment inside the DNA and avoid or reduce the accessibility of solvent molecules to complex. The emission titration behavior suggested that the complexes get into the hydrophobic environment inside the DNA, thereby avoid the quenching effect of solvent water molecules and the mobility of the complexes is restricted at the binding site ultimately leading to decrease in vibrational mode of relaxation [40].

4.4. Competitive DNA binding studies

Competitive binding studies using ethidium bromide (EB) bound to DNA could provide affluent information regarding the DNA binding nature and relative DNA binding affinity. EB is a well known pla-

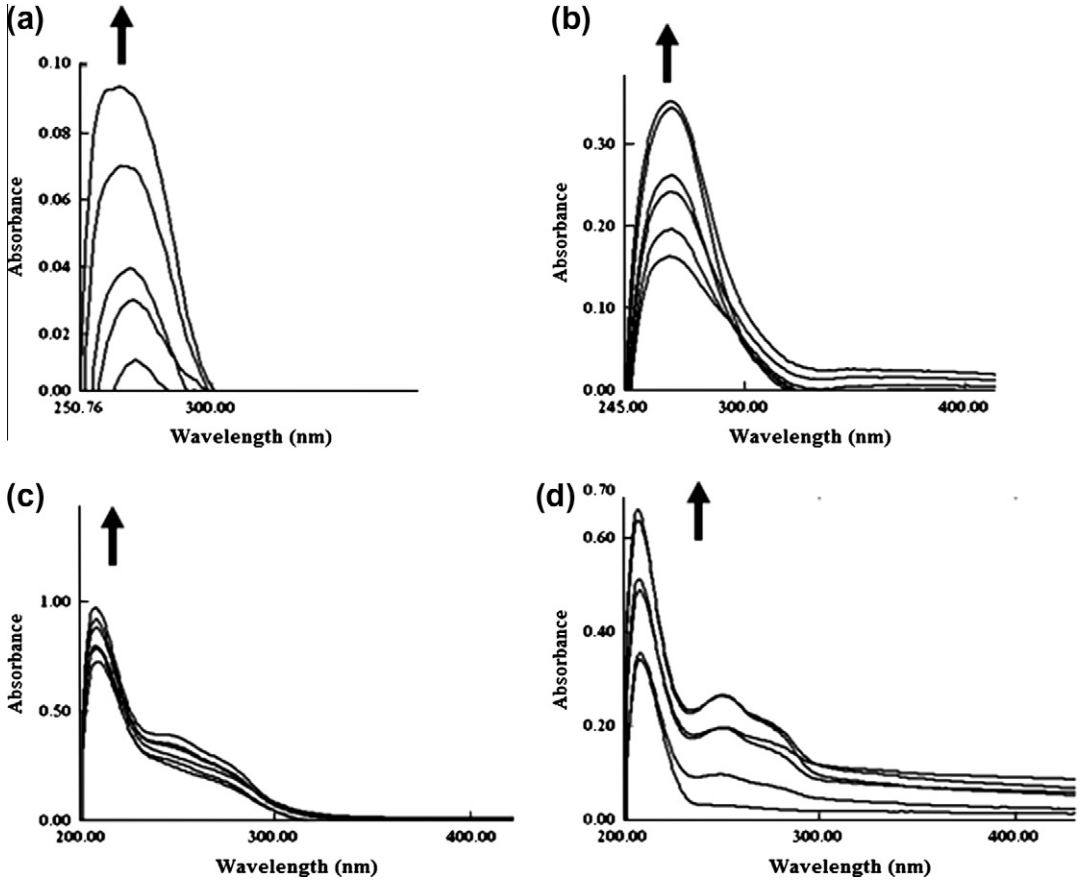

Fig. 2a. Absorption spectral traces of complexes in Tris HCl buffer (0.01 M, pH 7.2) upon addition of 5′-GMP, complexes **1** (a), **2** (b), **3** (c) and **4** (d) in the LF band.

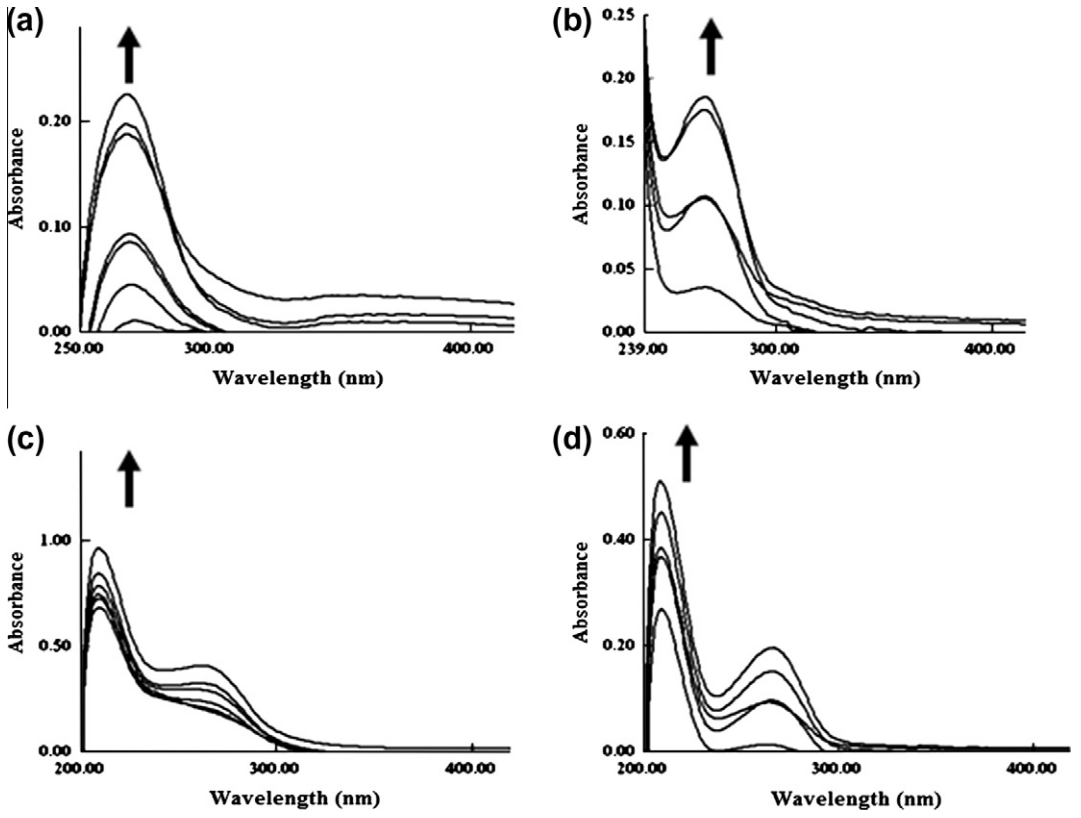

Fig. 2b. Absorption spectral traces of complexes in Tris HCl buffer (0.01 M, pH 7.2) upon addition of 5′-TMP, complexes **1** (a), **2** (b), **3** (c) and **4** (d) in the LF band.

Table 2
The binding constant (K_b) values of complexes **1**–**4** with 5′-GMP and 5′-TMP (mean standard deviation of ±0.06).

Complex	5′-GMP (M^{-1})	5′-TMP (M^{-1})
1	7.28×10^4	0.81×10^4
2	0.99×10^4	9.10×10^4
3	5.60×10^4	0.62×10^4
4	0.59×10^4	5.72×10^4

nar cationic dye widely used as a sensitive fluorescence probe for native DNA. EB emits intense fluorescence in the presence of DNA due to its strong intercalation between the adjacent DNA base pairs. The fluorescence intensity can be quenched by the addition of a second molecule due to the displacement of EB from DNA [41]. The fluorescence intensity of EB bound to DNA at 584 nm showed remarkable decreasing trend with increasing concentration of the complexes **1**–**4**. The resulting decrease in fluorescence is caused by EB changing from a hydrophobic environment to an aqueous environment by the displacement of EB from a DNA sequence by a quencher and the quenching is due to the reduction of the number of binding sites on the DNA that are available to the EB. As the peptide complexes were not expected to efficiently compete with the strong intercalator EB for the intercalative binding sites, the EB displacement mechanism was ruled out. So the decrease in intensity could be due to the interaction of the complexes to DNA through groove binding mode, releasing some EB molecules from EB-DNA system [42]. The quenching plots illustrated (Fig. 4) that the quenching of EB bound to CT-DNA by the peptide complexes are in good agreement with linear Stern–Volmer equation. From the quenching plots K_{sv} values were found to be 3.26, 1.01, 1.98 and 0.71 M^{-1} for complexes **1**–**4**, respectively.

4.5. Circular dichroic studies

Circular dichroism (CD) is a powerful method for distinguishing the three main DNA binding modes, namely intercalative (negative CD), outside groove binding (positive CD), and outside stacking (bisignate CD) [43,44]. The CD spectrum of calf thymus DNA consists of a positive band at 275 nm (UV, λ_{max} = 260 nm) caused by base stacking and a negative band at 245 nm caused by helicity, which are characteristic of DNA in right-handed B form. Intercalators are known to enhance the intensities of both positive and negative bands whereas groove binding and electrostatic interaction of complexes with DNA shows less or no perturbation on the base stacking and helicity bands [45]. Incubation of B-DNA with the peptide complexes induced marginal changes both in its positive and negative bands retaining the basic shape (Fig. 5). The change in the CD spectra confirms a binding event. In presence of complexes, the intensities of both the positive and negative bands decreased. The spectral behavior suggested that the DNA binding of the complexes induced certain conformational changes in which the more B-like conformation is transformed into a C-like structure

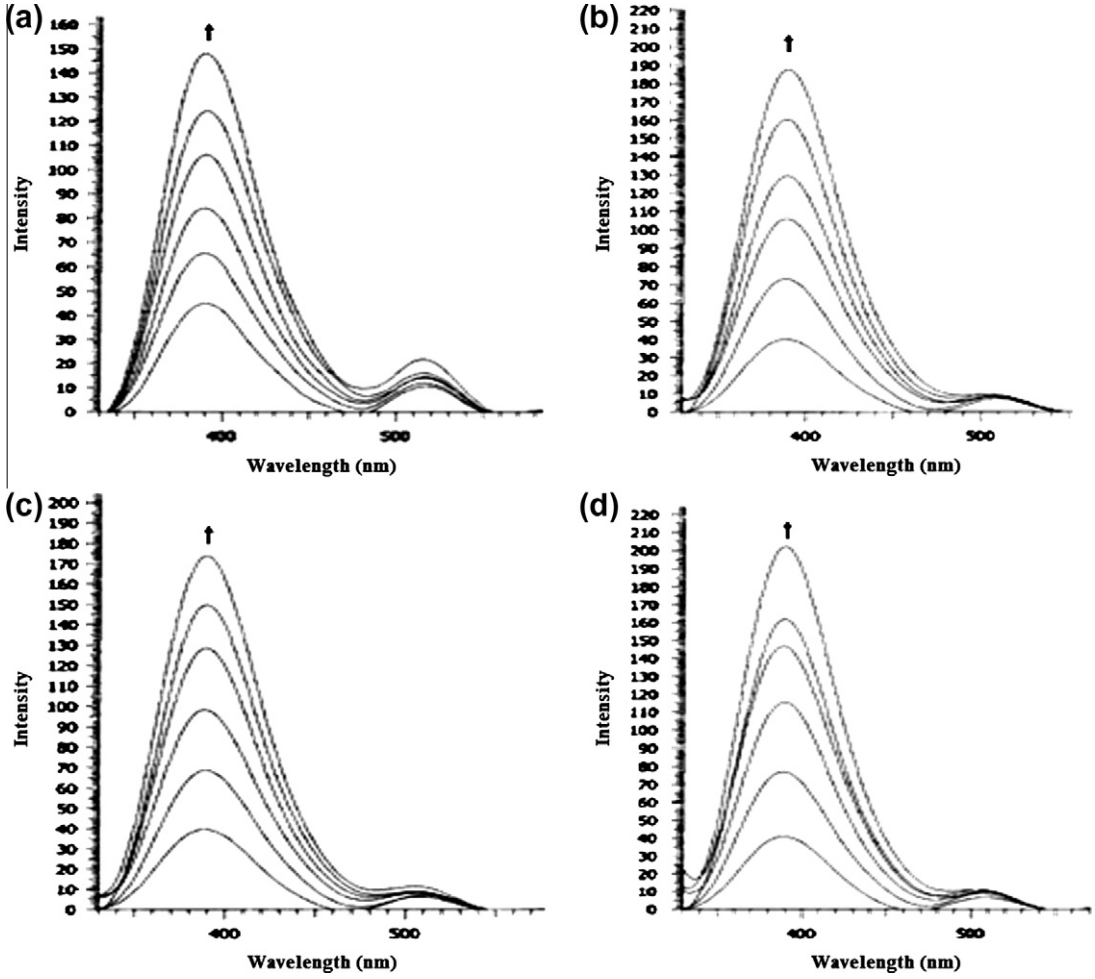

Fig. 3. Emission enhancement spectra of the complexes **1** (a), **2** (b), **3** (c) and **4** (d) with increasing concentration of complexes in the absence and presence of CT-DNA in Tris HCl buffer (0.01 M, pH 7.2). Arrows indicate change in intensity upon increasing concentration of CT-DNA.

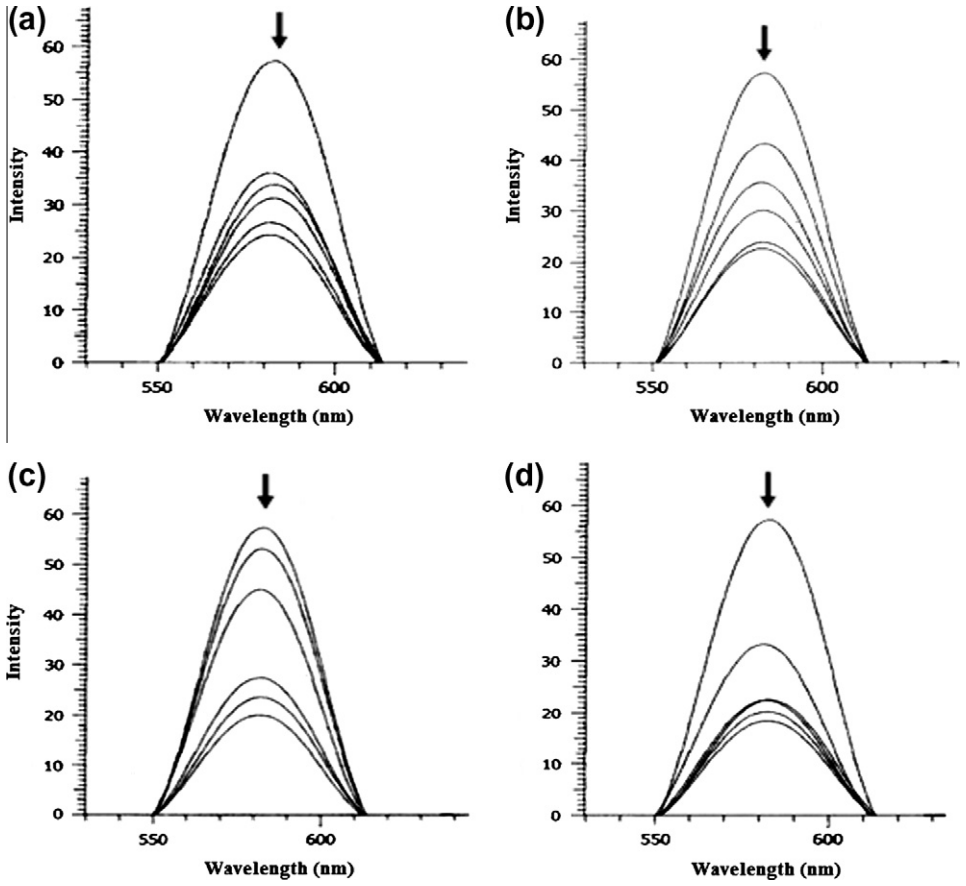

Fig. 4. Emission spectra of EB bound to DNA in the presence of complexes **1** (a), **2** (b), **3** (c) and **4** (d) in Tris HCl buffer. Arrows indicate the intensity changes upon increasing concentration of the complexes.

within the DNA molecule [46]. The CD spectral changes demonstrated a groove binding mode of interaction between the complexes and DNA.

4.6. Viscosity studies

To investigate further the binding nature of complexes to DNA, viscosity measurements with the solutions of DNA incubated with the complexes **1–4** have been carried out. The viscosity of DNA solution is sensitive to the addition of metal complexes which can bind to DNA. While classical intercalative mode causes a significant increase in viscosity of DNA solution due to separation of base pairs at intercalation sites and increase in overall DNA length, complexes those bind exclusively in the DNA grooves typically cause less positive or negative or no change in DNA viscosity [47]. The relative specific viscosity was calculated using the equation $((t - t_0)/t_0)$, where t_0 is the flow time for the buffer and t is the observed flow time for DNA in absence and presence of the complexes. The results were presented as (η/η_0) vs. binding ratio ([complex]/[DNA]), where η is the viscosity of DNA in the presence of complex and η_0 is the viscosity of DNA alone (Fig. 6). The relative specific viscosity of DNA decreased with increase in the concentration of the complexes **1–4**. The decrease in viscosity observed for the complexes suggested that the hydrophobic interaction of the peptide with DNA surface encouraged by the hydrogen bonding interactions lead to bending (kinking) of the DNA chain.

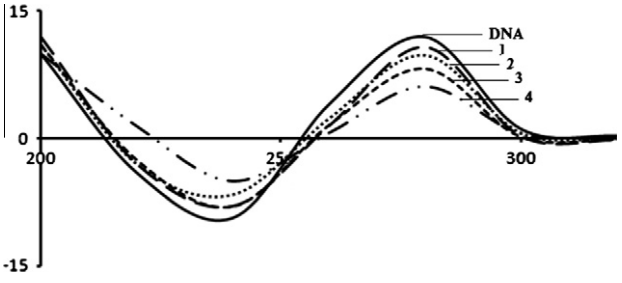

Fig. 5. CD spectrum of CT-DNA in absence and presence of complexes **1–4.**

4.7. Gel electrophoretic studies

To assess the DNA cleavage ability of the complexes supercoiled pBR322 DNA (300 ng) was incubated with varying concentration of complexes **1–4** in aqueous buffer solution (5 mM Tris HCl/50 mM NaCl, pH 7.2) for 0.5 h without addition of a reductant (Figs. 7 and S2). Upon gel electrophoresis of the reaction mixture, a concentration-dependent DNA cleavage was observed. With the increase in concentration of complexes, DNA was converted from supercoiled form (Form I) to nicked circular form (Form II) without further conversion to linear form (Form III) suggesting single strand DNA cleavage. Complex **1** exhibited higher cleavage. The DNA cleavage activity of complexes **1–4** in presence activators viz., H_2O_2, 3-mercaptopropionic acid (MPA), glutathione (GSH) and ascorbate (Asc) was significantly enhanced (Figs. 8 and S3). The activity efficacy followed the order H_2O_2 > MPA > Asc > GSH for complex **1**, H_2O_2 > MPA > GSH ≈ Asc for complex **2**, Asc > MPA≈GSH > H_2O_2 for complex **3** and H_2O_2 > MPA > GSH ≈ Asc for complex **4**. When the hydroxyl radical scavenger, DMSO (Figs. 8 and S3, Lane 6) and EtOH (Lane 7) were added to the complexes **1–4**, the nuclease activity was

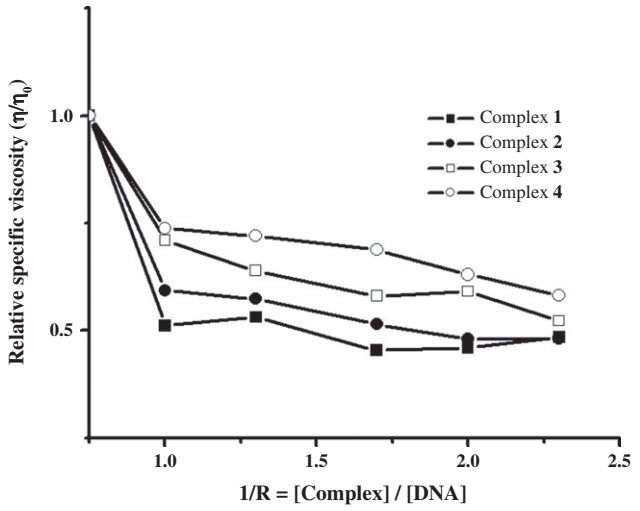

Fig. 6. Effect of increasing amounts of complexes **1, 2, 3** and **4** on the relative viscosity (η/η_0) of DNA in Tris HCl buffer (pH 7.2).

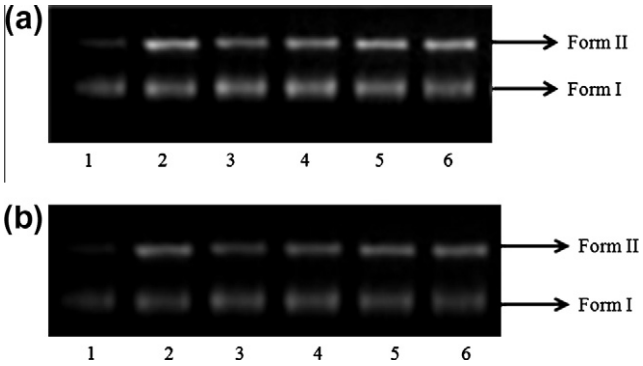

Fig. 7. (a) The cleavage patterns of the agarose gel electrophoresis for pBR322 plasmid DNA (300 ng) by **1** at 310 K after 30 min of incubation in buffer (5 mM Tris HCl/50 mM NaCl, pH = 7.2), Lane 1, DNA control; Lane 2, DNA + **1** (10 μM); Lane 3, DNA + **1** (20 μM); Lane 4, DNA + **1** (30 μM); Lane 5, DNA + **1** (40 μM); Lane 6, DNA + **1** (50 μM); (b) The cleavage patterns of the agarose gel electrophoresis for pBR322 plasmid DNA (300 ng) by **2** at 310 K after 30 min of incubation in buffer (5 mM Tris HCl/50 mM NaCl, pH = 7.2), Lane 1, DNA control; Lane 2, DNA + **2** (10 μM); Lane 3, DNA + **2** (20 μM); Lane 4, DNA + **2** (30 μM); Lane 5, DNA + **2** (40 μM); Lane 6, DNA + **2** (50 μM);

diminished indicating the involvement of OH^- radicals in the cleavage process. These OH^- radicals participate in the oxidation of the deoxyribose moiety, followed by hydrolytic cleavage of the sugar phosphate backbone. Further, the addition of singlet oxygen scavenger, NaN_3 to the reaction mixture scarcely inhibited the DNA cleavage (Lane 8) suggesting non-involvement of singlet oxygen as one of the ROS responsible for DNA breakage. In the case of SOD (superoxide radical scavenger) (Lane 9) the form II of the plasmid DNA was converted to form III indicating two subsequent and proximate single strand breaks of DNA non-randomly. The result demonstrated that superoxide radical is not responsible for DNA scission. The peptide moiety can also have an active role in the reduction of Cu(II). Based on the above results, it could be concluded that the hydroxyl radicals are responsible for the DNA cleavage. These OH^- radicals participate in the oxidation of the deoxyribose moiety, followed by hydrolytic cleavage of the sugar phosphate backbone.

The initial step of the possible reaction mechanisms of DNA damage by Cu(II) complexes in the presence of hydrogen peroxide is the interaction of Cu(II) complex with the outer sphere of DNA strand. The second step is the reduction of Cu(II) complex to Cu(I) complex by reducing agent, then the Cu(I)–DNA adduct

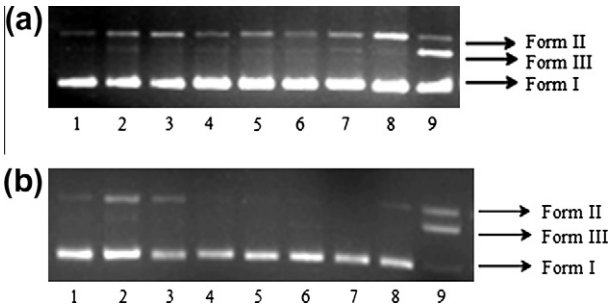

Fig. 8. (a) Agarose gel electrophoresis pattern for the cleavage pattern of pBR322 plasmid DNA (300 ng) by complex **1** (50 μM) in the presence of different activating agents at 310 K after incubation for 30 min. Lane 1, DNA control; Lane 2, DNA + **1** + H_2O_2 (0.4 μM); Lane 3, DNA + **1** + MPA (0.4 μM); Lane 4, DNA + **1** + GSH (0.4 μM); Lane 5, DNA + **1** + Asc (0.4 μM); Lane 6, DNA + **1** + DMSO (0.4 μM); Lane 7, DNA + **1** + EtOH (0.4 μM); Lane 8, DNA + **1** + NaN_3 (0.4 μM); Lane 9, DNA + **1** + Superoxide Dismutase (15 Units); (b) Agarose gel electrophoresis pattern for the cleavage pattern of pBR322 plasmid DNA (300 ng) by complex **2** (50 μM) in the presence of different activating agents at 310 K after incubation for 30 min. Lane 1, DNA control; Lane 2, DNA + **2** + H_2O_2 (0.4 μM); Lane 3, DNA + **2** + MPA (0.4 μM); Lane 4, DNA + **2** + GSH (0.4 μM); Lane 5, DNA + **2** + Asc (0.4 μM); Lane 6, DNA + **2** + DMSO (0.4 μM); Lane 7, DNA + **2** + EtOH (0.4 μM); Lane 8, DNA + **2** + NaN_3 (0.4 μM); Lane 9, DNA + **2** + Superoxide Dismutase (15 Units).

further reacts with H_2O_2 via Fenton mechanism to generate a hydroxyl radical species that can bind to the metal ion [48]:

$$\text{Cu(II)complex} + \text{DNA} \rightarrow \text{Cu(II)} - \text{DNA}$$

$$\text{Cu(II)} - \text{DNA} \rightarrow \text{Cu(I)} - \text{DNA}$$

$$\text{Cu(I)} - \text{DNA} + \text{H}_2\text{O}_2 \rightarrow \text{Cu(II)}(\cdot\text{OH}) - \text{DNA} + \cdot\text{OH}$$

The Cu-peptide complexes could permit molecular oxygen to generate an α-carbon stabilized radical from the C-terminal amino acid present in the peptidic structure. Later, a redox reaction between this radical and the nearby Cu(II) would yield Cu(I) which further cleaves the DNA [49].

In the complexes **1–4** the DNA cleavage is inhibited remarkably with major groove binding agent, methyl green (Figs. 9 and S4, Lane 2). However, no apparent inhibition of DNA damage was observed in presence of DAPI, minor groove binding agent (Fig. 9, Lane 3). This suggests major groove preference for the complexes. This is in support of the findings from UV–vis absorption titration that the complexes can form hydrogen bonds via amine group of

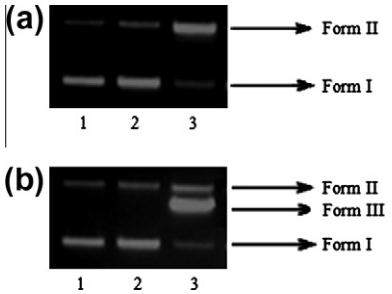

Fig. 9. (a) The cleavage patterns of the agarose gel electrophoresis for pBR322 plasmid DNA (300 ng) by **1** in the presence of DNA major groove binding agent methyl green and minor groove binding agent, DAPI at 310 K after 30 min of incubation in buffer (5 mM Tris HCl/50 mM NaCl, pH = 7.2), Lane 1, DNA control; Lane 2, DNA + **1** + Methyl green; Lane 3, DNA + **1** + DAPI; (b) The cleavage patterns of the agarose gel electrophoresis for pBR322 plasmid DNA (300 ng) by **2** in the presence of DNA major groove binding agent, methyl green and minor groove binding agent DAPI at 310 K after 30 min of incubation in buffer (5 mM Tris HCl/50 mM NaCl, pH = 7.2), Lane 1, DNA control; Lane 2, DNA + **2** + Methyl green; Lane 3, DNA + **2** + DAPI.

Table 3
Summary of the screening data of **1** against different tumor cells.

Cell line	A498	A549	Zr-75-1	HT29	A2780	SiHa	MCF7	
GI_{50}	1	29.9	67.6	>80	>80	31.2	77.9	>80
	ADR	<10	<10	<10	<10	<10	<10	<10
TGI	1	56.5	122.2	>80	>80	62.7	>80	>80
	ADR	17.4	58.0	54.8	29.6	18.4	49.5	25.9
LC_{50}	1	>80	176.8	>80	>80	>80	>80	>80
	ADR	41.4	116.4	107.3	57.2	57.1	>80	60.1

GI_{50} = Growth inhibition of 50% (GI_{50}) calculated from $[(Ti–Tz)/(C–Tz)] \times 100 = 50$, drug concentration result in a 50% reduction in the net protein increase.
GI_{50} value < 10 μg/mL is considered to demonstrate activity.

peptide moiety with N-3 of adenine or O-2 of thymine in the DNA at the major groove. Major groove binding is particularly attractive because in biological systems the sequence specific code recognition mostly occurs by interaction between the DNA major groove and specific protein surface motifs. The major groove offers a number of potential H-bond interaction sites to which protein motifs can selectively bind.

5. Antitumor activity

In vitro antitumor activity of **1** in terms of GI_{50} (concentration of drug required to decrease the cell growth to 50%, compared with that of the untreated cell number), TGI (concentration of drug required to decrease the cell growth to 100%, compared with that of the untreated cell number during drug incubation) and LC_{50} (concentration of drug required to decrease the cell growth by 50% of the initial cell number prior to the drug incubation) values were tested against A498 (Renal cell), A549 (Lung), Zr-75-1 (Breast), HT29 (Colon adenocarcinoma grade II cell line), A2780 (Ovary), SiHa (Uterine cervix) and MCF7 (Human breast) by SRB assay. Complex **1** exhibited moderate results against A498 (Renal cell) and A2780 (Ovary). The results are presented in Table 3.

6. Conclusion

The dipeptides Boc-Val-Pro-OMe (L_1), Boc-Ala-Pro-OMe (L_2) and their Cu(II) and Zn(II) complexes **1**–**4** were synthesized owing to the fact that metallopeptide systems are unique and can affect the biological activity of peptides. The thermodynamic stability of metallopeptides can lead to the recognition of some peptides as ligands competitive to other ligands present in human body fluids. The characterization of these complexes was determined by elemental analysis, and other spectroscopic techniques viz., IR, NMR, ESI–MS, UV–vis and EPR. I*n vitro* DNA-binding profile of these metallopeptide complexes was studied by various optical (absorption, fluorescence, CD spectroscopy), and hydrodynamic methods. The *in vitro* DNA-binding studies of the complexes studied by absorption, fluorescence, circular dichroic spectral and viscosity measurements revealed binding of the complexes via groove binding mode to the DNA double helix. The absorption studies of peptide complexes with mononucleotides performed to assess the base specific interaction of the metal ions revealed higher propensity of Cu(II) complexes for 5′-GMP and Zn(II) complexes to 5′-TMP. Interaction between the peptide complexes **1** and **2** with pBR322 DNA evaluated by agarose gel electrophoresis exhibited profound efficiency to cleave plasmid DNA and the cleavage mechanism involved a hydrolytic mechanistic pathway. The cleavage patterns observed in presence of groove recognition agents; DAPI and methyl green support the major groove binding mode of the complexes. The present study proposes metallopeptide Cu(II) and Zn(II) complexes as new and better DNA-binding and DNA-cleaving agents.

Therefore, i*n vitro* antitumor activity of **1** was evaluated by SRB assay, which exhibited moderate results against A498 (Renal Cell) and A2780 (Ovary). The studies revealed that the peptide complexes exhibited apoptotic activity in addition to DNA binding property. The design of peptide complexes could fulfill the criteria for efficacious metal-based drugs exhibiting reduced systemic toxicity and base specificity towards the cancerous cells. These metal–peptide complexes warrant their future as potential cancer chemotherapeutic agents.

Acknowledgments

The authors are thankful to Sophisticated Test and Instrumentation Centre, Cochin University, Cochin, India for providing elemental analysis, Sophisticated Analytical Instrumentation Facility, Panjab University, Chandigarh, India for providing NMR spectra, Regional Sophisticated Instrumentation Center, Central Drug Research Institute, Lucknow, India for providing ESI–MS, Advanced instrumentation research facility, Jawaharlal Nehru University, Delhi, India for providing CD facility and Advanced Centre for Treatment, Research and Education in Cancer, Kharghar, Navi Mumbai for carrying out antitumor activity.

Appendix A. Supplementary material

Supplementary data associated with this article can be found, in the online version, at http://dx.doi.org/10.1016/j.jphotobiol.2012.12.009.

References

[1] J.C. Mai, Z. Mi, S.-H. Kim, B. Ng, P.D. Robbins, A proapoptotic peptide for the treatment of solid tumor, Cancer Res. 61 (2001) 7709–7712.
[2] A. Risso, E. Braidot, M.C. Sordano, A. Vianello, F. Marci, B. Skerlavaj, BMAP-28, an antibiotic peptide of innate immunity, induces cell death through opening of the mitochondrial permeability transition pore, Mol. Cell. Biol. 22 (2002) 1926–1935.
[3] R.A. Cruciani, J.L. Barker, M. Zasloff, H.C. Chen, O. Colamonici, Antibiotic magainins exert cytolytic activity against transformed cell lines through channel formation, Proc. Natl. Acad. Sci. USA 88 (1991) 3792–3796.
[4] S.A. Johnstone, K. Gelmon, L.D. Mayer, R.E. Hancock, M.B. Bally, *In vitro* characterization of the anticancer activity of membrane-active cationic peptides. I. Peptide-mediated cytotoxicity and peptide-enhanced cytotoxic activity of doxorubicin against wild-type and p-glycoprotein over-expressing tumor cell lines, Anticancer Drug Des. 15 (2000) 151–160.
[5] F.J. Sharom, G. DiDiodota, X. Yu, K.J.D. Ashbourne, Interaction of the p-glycoprotein multidrug transporter with peptides and ionophores, J. Biol. Chem 270 (1995) 10334–10341.
[6] M. Demeunynck, C. Bailly, W.D. Wilson, Small molecules, DNA and RNA Binders; From Synthesis to Nucleic Acid Complexes, Wiley-VCH, Weinheim, 2002.
[7] Y. Jin, M.A. Lewis, N.H. Gokhale, E.C. Long, J.A. Cowan, Influence of stereochemistry and redox potentials on the single- and double-strand DNA cleavage efficiency of Cu(II) and Ni(II)·Lys-Gly-His-Derived ATCUN metallopeptides, J. Am. Chem. Soc. 129 (2007) 8353–8361.
[8] K. Karidi, J. Reedijk, N. Hadjiliadis, A. Garoufis, Synthesis, characterization and DNA binding properties of oligopyridine–ruthenium(II)-amino acid conjugates, J. Inorg. Biochem. 101 (2007) 1483–1491.
[9] A. Myari, N. Hadjiliadis, A. Garoufis, Synthesis and characterization of the diastereomers Λ-and Δ-$[Ru(bpy)_2$ (m-bpy- L -Arg-Gly-L -Asn- L -Ala-L -His-L -Glu-L -Arg)$]Cl_2$ ^{1}H NMR studies on their interactions with the deoxynucleotide duplex d[(5′-GCGCTTAAGCGC-3′)$_2$] and d[(5′-CGCGA TCGCG-3′)$_2$], J. Inorg. Biochem. 99 (2005) 616–626.
[10] M.P. Fitzsimons, J.K. Barton, Design of a synthetic nuclease: DNA hydrolysis by a zinc-binding peptide tethered to a rhodium intercalator, J. Am. Chem. Soc. 119 (1997) 3379–3380.
[11] C.A. Hastings, J.K. Barton, Perturbing the DNA sequence selectivity of metallointercalator-peptide conjugates by single amino acid modification, Biochemistry 38 (1999) 10042–10051.
[12] J.B. Blanco, V.I. Dodero, M.E. Vázquez, M. Mosquera, L. Castedo, J.L. Mascarenas, Sequence-specific DNA binding by noncovalent peptide–tripyrrole conjugates, Angew. Chem. Int. Ed. 45 (2006) 8210–8214.
[13] H. Sigel (Ed.), Metal Ions in Biological Systems, vol. 13, Marcel Dekker, New York, 1981.

[14] T. Miura, A. Horii, H. Mototani, H. Takeuchi, Raman spectroscopic study on the copper(II) binding mode of prion octapeptide and its pH dependence, Biochemistry 38 (1999) 11560–11569.
[15] M. Gelinsky, H. Vahrenkamp, Zinc complexes of a helical 22-mer peptide with two histidine donors, Eur. J. Inorg.Chem. (2002) 2458–2462.
[16] H. Boerzel, M. Koeckert, W. Bu, B. Spingler, S.J. Lippard, Zinc-bound thiolate–disulfide exchange: a strategy for inhibiting metallo-β-lactamases, Inorg. Chem. 42 (2003) 1604–1615.
[17] N.P. Pauletich, C.O. Pabo, Zinc finger-DNA recognition: crystal structure of a Zif268-DNA complex at 2.1 A, Science 252 (1991) 809–817.
[18] Q. Lin, C.F. Barbas, P.G. Schultz, Small-molecule switches for zinc finger transcription factors, J. Am. Chem. Soc. 125 (2003) 612–613.
[19] A. Wolfe, G.H. Shimer, T. Meehan, Polycyclic aromatic hydrocarbons physically intercalate into duplex regions of denatured DNA, Biochemistry 26 (1987) 6392–6396.
[20] J.R. Lakowicz, G. Weber, Quenching of fluorescence by oxygen. A probe for structural fluctuations in macromolecules, Biochemistry 12 (1973) 4161–4170.
[21] F. Arjmand, A. Jamsheera, Synthesis, characterization and *in vitro* DNA binding studies of tin(IV) complexes of tert-butyl 1-(2-hydroxy-1-phenylethylamino)-3-methyl-1-oxobutan-2-ylcarbamate, J. Organomet. Chem. 696 (2011) 3572–3579.
[22] P. Skehan, R. Storeng, D. Scudiero, A. Monks, J. McMahon, D. Vistica, J.T. Warren, H. Bokesch, S. Kenney, M.R. Boyd, New colorimetric cytotoxicity assay for anticancer-drug screening, J. Natl. Cancer Inst. 82 (1990) 1107–1112.
[23] M. Bodanszky, A. Bodanszky, The Practice of Peptide Synthesis, Springer-Verlag, New York, 1984. pp. 1–282.
[24] P.R. Reddy, N. Raju, B. Satyanarayana, Synthesis, characterization, and DNA binding and cleavage properties of copper(II)-tryptophanpenylalanine-1,10-phenanthroline/2,2′-bipyridine complexes, Chem. Biodiv. 8 (2011) 131–144.
[25] J.-H. Choi, Y.P. Hong, Y.C. Park, S.H. Lee, K.S. Ryoo, Synthesis and spectral properties of [N-(2-aminoethyl)-1,2-ethanediamine] (L-prolylglycinato) chromium(III) Perchlorate, Bull. Korean Chem. Soc. 22 (2001) 107–109.
[26] D.D. Stamenovi, S.R. Trifunovi, The synthesis and characterization of facial and meridional isomers ofuns-cis-(ethylenediamine-N-N'-di-3-propionato)cobalt (III) complexes with S-lysine and S-histidine, J. Serb. Shem. Soc. 67 (2002) 235–241.
[27] L.H. Abdel-Rahman, L.P. Battaglia, M.R. Mahmoud, Synthesis, characterization and stability constant determination of L-phenylalanine ternary complexes of cobalt(II), nickel(II), copper(II) with N-heterocyclic aromatic bases and x-ray crystal structure of aqua-1,10-phenanthroline-l-phenylalaninatocopper(II) perchlorate complex, Polyhedron 15 (1996) 327–334.
[28] S. Chandra, Sangeethika, S. Thakur, Electronic, e.p.r., cyclic voltammetric and biological activities of Copper(II) complexes with macrocyclic ligands, Trans. Met. Chem. 29 (2004) 925–935.
[29] N. Raman, S. Ravichandran, C. Thangaraja, Copper(II), cobalt(II), nickel(II) and zinc(II) complexes of Schiff base derived from benzil-2,4-dinitrophenyl hydrazone with aniline, J. Chem. Sci. 116 (2004) 215–219.
[30] S. Rajalakshmi, T. Weyhermüller, A.J. Freddy, H.R. Vasanthi, B.U. Nair, Anomalous behavior of pentacoordinate copper complexes of dimethylp henanthroline and derivatives of terpyridine ligands: studies on DNA binding, cleavage and apoptotic activity, Eur. J. Med. Chem. 46 (2011) 608 –617.
[31] A.A. Jain, M.R. Rajeshwari, Binding studies on peptide – oligonucleotide complex: intercalation of tryptophan in GC-rich region of c-myc gene, Biochim. Biophys. Acta 1622 (2003) 73–81.
[32] R. Nagane, T. Koshigoe, M. Chikira, Interaction of Cu(II)-Arg-Gly-His-Xaa metallopeptides with DNA: effect of C-terminal residues, Leu and Glu, J. Inorg. Biochem. 91 (2003) 204–212.
[33] P.R. Reddy, S.K. Mohan, K.S. Rao, Ternary Zinc(II)-dipeptide complexes for the hydrolytic cleavage of DNA at physiological pH, Chem. Biodiv. 2 (2005) 672–683.
[34] P.R. Reddy, P. Manjula, S.K. Mohan, Novel peptide-based copper(II) complexes for total hydrolytic cleavage of, DNA 2 (2005) 1338–1350.
[35] F. Arjmand, S. Parveen, D.K. Mohapatra, Synthesis, characterization of Cu(II) and Zn(II) complexes of proline–glycine and proline–leucine tetrapeptides:In vitro DNA binding and cleavage studies, Inorg. Chim. Acta 388 (2012) 1–10.
[36] L. Lomozik, A. Gosowska, G. Krzysko, Interactions of 1,12-diamino-4,9-dioxadodecane (OSpm) and Cu(II) ions with pyrimidine and purine nucleotides: Adenosine-5-monophosphate (AMP) and cytidine-5-monophosphate (CMP), J. Inorg. Biochem. 100 (2006) 1781–1789.
[37] M.-H. Baik, R.A. Friesner, S.J. Lippard, Theoretical study of cisplatin binding to purine bases: why does cisplatin prefer guanine over adenine?, J Am. Chem. Soc. 125 (2003) 14082–14092.
[38] S. Aoki, E. Kimura, Highly selective recognition of thymidine mono- and diphosphate nucleotides in aqueous solution by ditopic receptors Zinc(II)-bis(cyclen) complexes (cyclen = 1,4,7,10-tetraazacyclododecane), J. Am. Chem. Soc. 122 (2000) 4542–4548.
[39] B.L. Hauenstein, W.J. Dressick, S.L. Buell, J.N. Demas, B.A. De-Graff, A new probe of solvent accessibility of bound photosensitizers. I. Ruthenium(II) and osmium(II) photosensitizers in sodium lauryl sulfate micelles, J. Am. Chem. Soc. 105 (1983) 4251–4255.
[40] L.-F. Tan, H. Chao, K.-C. Zhen, J.-J. Fei, F. Wang, Y.-F. Zhou, L.-N. Ji, Effects of the ancillary ligands of polypyridyl Ruthenium(II) complexes on the DNA-binding and photocleavage behaviors, Polyhedron 26 (2007) 5458–5468.
[41] R. Indumathy, S. Radhika, M. Kanthimathi, T. Weyhermuller, B.U. Nair, Cobalt complexes of terpyridine ligand: Crystal structure and photocleavage of DNA, J. Inorg. Biochem. 101 (2007) 434–443.
[42] D.L. Boger, B.E. Fink, S.R. Brunette, W.C. Tse, M.P. Hedrick, A simple, high-resolution method for establishing DNA binding affinity and sequence selectivity, J. Am. Chem. Soc. 123 (2001) 5878–5891.
[43] N. Grover, N. Gupta, P. Singh, H.H. Thorp, Studies of electrocatalytic DNA cleavage by oxoruthenium(1V). X-ray crystal structure of [Ru(tpy)(tmen)OH2](C104)2(tmen = N, N, N′, N′-tetramethylethylenediamine; tpy = 2,2′,2″-terpyridine), Inorg. Chem. 31 (1992) 2014–2020.
[44] R.F. Pasternack, Circular dichroism and the interactions of water soluble porphyrins with DNA—a mini review, Chirality 15 (2003) 329–332.
[45] K. Karidi, A. Garoufis, A. Tsipis, N. Hadjiliadis, H. Dulk, J. Reedijik, Synthesis, characterization, *in vitro* antitumor activity, DNA-binding properties and electronic structure (DFT) of the new complex *cis*-(Cl, Cl)[$Ru^{II}Cl_2(NO^+)$(terpy)]Cl, Dalton. Trans. (2005) 1176–1187.
[46] S. Mahadevan, M. Palaniandavar, Spectroscopic and voltammetric studies on copper complexes of 2,9-dimethyl-1,10-phenanthrolines bound to calf thymus DNA, Inorg. Chem. 37 (1998) 693–700.
[47] U. Chaveerach, A. Meenongwa, Y. Trongpanich, C. Soikum, P. Chaveerach, DNA binding and cleavage behaviors of Copper (II) complexes with amidino-O-methylurea and N-methylphenyl-amidino-O-methylurea, and their anti bacterial activities, Polyhedron 29 (2010) 731–738.
[48] K. Karidi, A. Garoufis, N. Hadjiliadis, J. Reedijk, Solid-phase synthesis, characterization and DNA binding properties of the first chloro(polypyridyl) ruthenium conjugated peptide complex, Dalton Trans. (2005) 728–734.
[49] A. Garcia-Raso, J.J. Fiol, B. Adrover, V. Moreno, I. Mata, E. Espinosa, E. Molins, Synthesis, structure and nuclease properties of several ternary copper(II) peptide complexes with 1,10-phenanthroline, J. Inorg. Biochem. 95 (2003) 77–86.